Some Progress on New Double-Folding Potential, α-α Elastic Scattering, etc

Dong BAI

School of Physics Science and Engineering, Tongji University

Sep 3, 2019

Talk given at **ECT* Workshop on "Light clusters in nuclei and nuclear matter: Nuclear structure and decay, heavy-ion collisions, and astrophysics"**, Trento, Italy

Outline

Introduction

Binary Cluster Models

Many α-cluster states could be studied within the **binary cluster models** (a.k.a. local potential approach, extreme cluster models, potential model, etc).

Applications:

1. **Structural and decay properties of parent nucleus $= \alpha +$ doubly magic core**:
   $^{8}Be = \alpha + \alpha$, $^{20}Ne = \alpha + {}^{16}O$, $^{44}Ti = \alpha + {}^{40}Ca$, $^{104}Te = \alpha + {}^{100}Sn$, $^{212}Po = \alpha + {}^{208}Pb$.
2. α decays in medium-mass, heavy, and superheavy nuclei:
   systematic studies along various isotopic and isotonic chains, α-decay fine structures, etc.
3. Potential-model approach to nuclear reaction problems:
   elastic scattering, inelastic scattering, fusion reactions, etc.

D. S. Delion, *Theory of Particle and Cluster Emission* (2010).
D. S. Delion, Z. Ren, A. Dumitrescu, D. Ni (2018).
I. Thompson, F. M. Nunes (2009).
K. Hagino, N. Takigawa (2012).

Parent Nucleus $= \alpha +$ Doubly Magic Core:

Binary cluster models have been applied successfully to study α-cluster structures in parent nucleus $= \alpha +$ doubly magic core, giving a unified description of the energy spectrum, electromagnetic transitions, α decays, nuclear sizes, etc.

Three essentials:

1. relevant degrees of freedoms $= \alpha$ cluster $+$ spherical doubly magic core;
2. *Wildermuth condition* used to implement Pauli blocking between the α cluster and the core nucleus;
3. **effective potentials between the α cluster and the core nucleus:**
   $\times$: squared-well potential, cosh potential, Woods-Saxon (WS) potential, **double-folding potential**, etc.
   $\surd$: WS+WS^3 potential, **Woods-Saxon-Gaussian (WSG) potential**, (WS+WS^3)$\times$(1+Gaussian) potential, etc.

Q: What's the microscopic origin of the WSG potential?

A: Perhaps closely related to Pauli blocking.

Non-Localized Cluster Model

Non-localized cluster model is proposed by Bo Zhou, Y. Funaki, H. Horiuchi, Zhongzhou Ren, G. Röpke, P. Schuck, A. Tohsaki, Chang Xu, T. Yamada in 2012-2014, and generalizes the key insights behind α-**particle condensates** of THSR (**T**ohsaki-**H**oriuchi-**S**chuck-**R**öpke).

The non-localized cluster model is based on the new picture of **non-localized clustering**, which is different from the traditional picture of **localized clustering**.

Local Clustering

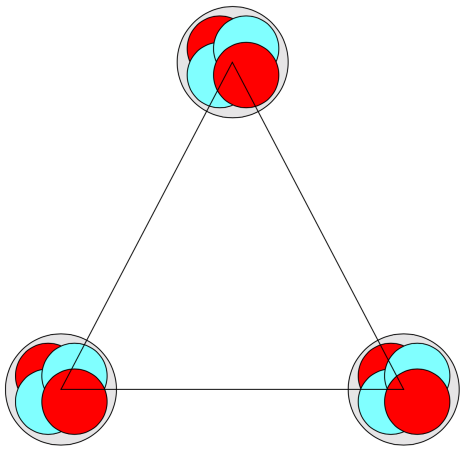

$^{12}C = \alpha + \alpha + \alpha$

Non-Local Clustering

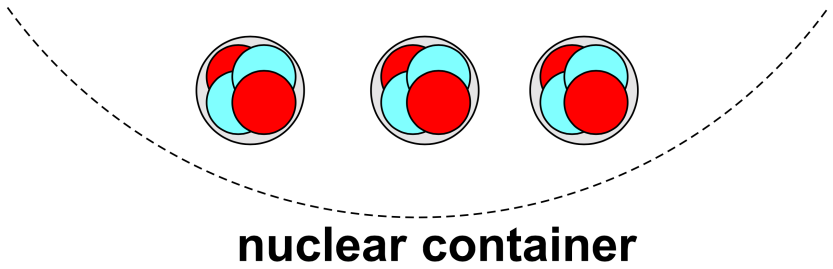

The non-localized cluster model has been used to study structural properties of α-cluster states in various nuclei and hypernuclei, including

- ^{6,8}He, $^{8-12}$Be, ^{9,10}B, ^{10,12}C, ^{16}O, ^{20}Ne;
- ${}^{9}_{\Lambda}$Be, ${}^{13}_{\Lambda}$C.

  Y. Funaki, H. Horiuchi, A. Tohsaki (2015).
  M. Freer, H. Horiuchi, Y. Kanada-En'yo, D. Lee, Ulf-G. Meißner (2018).
  Bo Zhou, Y. Funaki, H. Horiuchi, A. Tohaski (2019).

Further Direction:

Generalize non-localized cluster model to **nuclear reactions**.
Take the α-α elastic scattering as the first step.

New Double-Folding Potential from the Brink Wave Function

Woods-Saxon-Gaussian Potential

Within the framework of the binary cluster model,
the WSG potential + Coulomb potential + centrifugal potential
could give a reliable description of the effective potential between the α cluster and the core nucleus,

$$V_N(r) = -\frac{V_0}{1+\exp[(r-R)/a]}\{1+\alpha\exp[-\beta(r-R)^2]\}, \tag{1}$$

$$V_C(r) = \begin{cases} \frac{Z_c Z_\alpha e^2}{r}, & r \geq R, \\ \frac{Z_c Z_\alpha e^2}{2R}\left[3-\left(\frac{r}{R}\right)^2\right], & r < R, \end{cases} \tag{2}$$

$$V_L(r) = \frac{\hbar^2}{2\mu r^2}\left(L+\frac{1}{2}\right)^2. \tag{3}$$

The free parameters in the WSG potential are determined by fitting the energy spectrum of parent nucleus = α+doubly magic core,

$$V_0 = 203.3 \text{ MeV}, \quad a = 0.73 \text{ fm}, \quad \alpha = -0.478, \quad \beta = 0.054 \text{ fm}^{-2}.$$
$$R_D(^{20}\text{Ne}) = 3.25 \text{ fm}, \quad R_D(^{44}\text{Ti}) = 4.61 \text{ fm}, \quad R_D(^{212}\text{Po}) = 6.73 \text{ fm}. \tag{4}$$

Wildermuth Condition

used to implement partially the Pauli blocking between the α cluster and the core nucleus, imposing selection rules on the number n of the nodes in the wave function through the global quantum number $G = 2n + L$, with

$$G(^{20}\mathrm{Ne}) = 8, \quad G(^{44}\mathrm{Ti}) = 12, \quad G(^{212}\mathrm{Po}) = 18. \tag{5}$$

^{20}Ne:

J^π	E_{exp} [MeV]	E_{th} [MeV]	$B(\mathrm{E2}\downarrow)_{\mathrm{exp}}$ [W.u.]	$B(\mathrm{E2}\downarrow)_{\mathrm{th}}$ [W.u.]	R_i [fm]
0^+	0.000	1.196	–	–	4.14
2^+	1.634	2.320	20.3 ± 1.0	18.3	4.13
4^+	4.248	4.529	22.0 ± 2.0	23.7	4.04
6^+	8.776	7.706	20.0 ± 3.0	19.3	3.83
8^+	11.951	11.764	9.03 ± 1.3	9.9	3.50

Standard Double-Folding Potential

Traditionally, the double-folding potential is given by

$$U(\mathbf{r}) = \lambda \int \mathrm{d}\mathbf{r}_A \mathrm{d}\mathbf{r}_a \rho_c(\mathbf{r}_A)\rho_\alpha(\mathbf{r}_a) V_{\mathrm{NN}}(\mathbf{r} + \mathbf{r}_A - \mathbf{r}_a), \tag{6}$$

with $\rho_c(\mathbf{r}_A)$ and $\rho_\alpha(\mathbf{r}_a)$ being the density profiles of the core nucleus and the α cluster, $V_{NN}(\mathbf{r})$ being the M3Y effective potential, and $\lambda \sim 0.5$ being the renormalization factor.

The density profile of the α cluster is often taken to be of the Gaussian shape

$$\rho_\alpha(r_a) = 0.4299 \exp(-0.7024 r_a^2), \tag{7}$$

with parameters determined by the electron-scattering data.

The density profiles $\rho_\alpha(\mathbf{r}_a)$ and $\rho_c(\mathbf{r}_A)$ are **frozen** as the α cluster approaches the core nucleus from the infinity.

^{212}Po

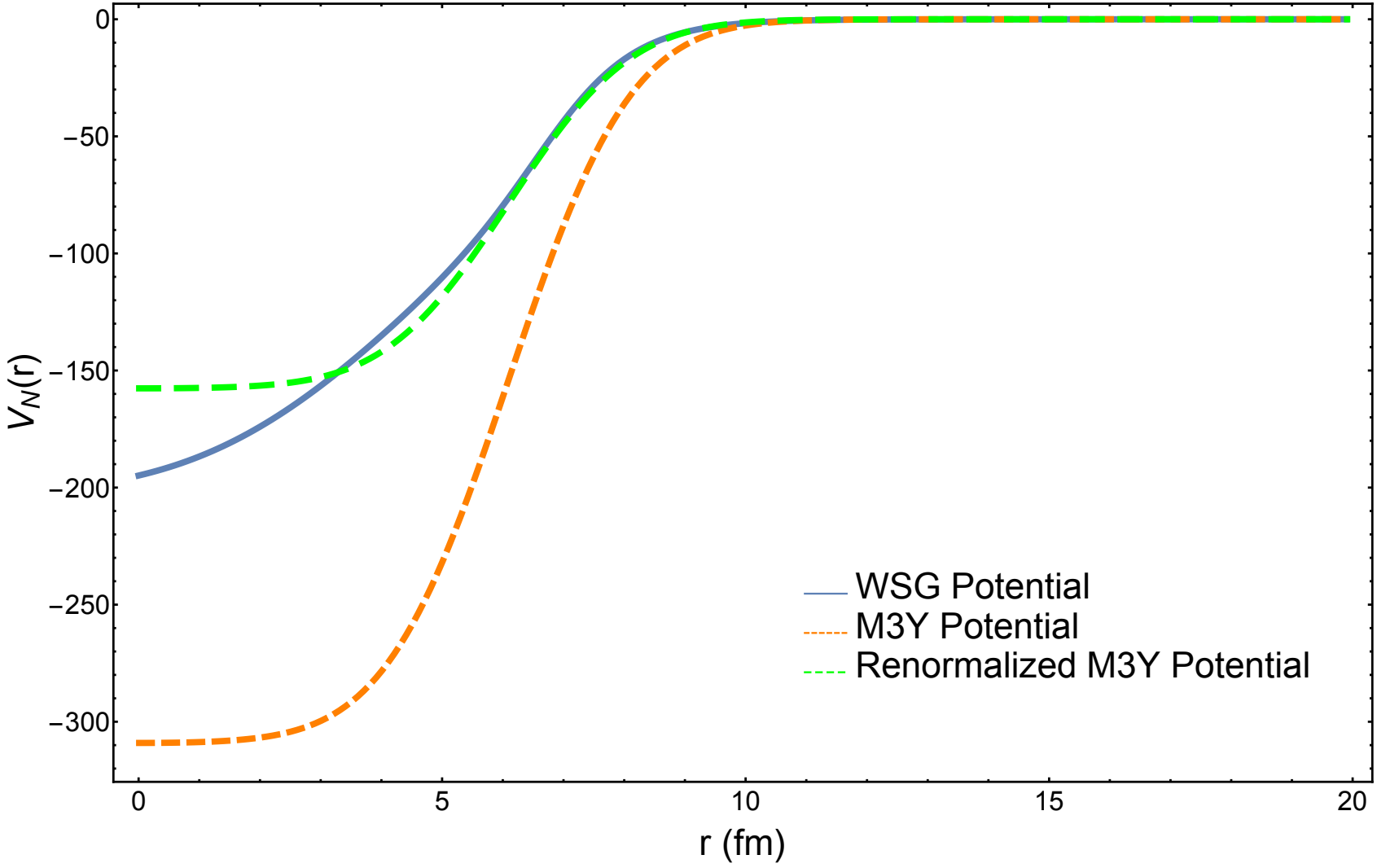
0
−50
−100
−150
−200
−250
−300
V_N(r)
0
5
10
15
20
r (fm)
WSG Potential
M3Y Potential
Renormalized M3Y Potential

New Double-Folding Potential

Recent studies on quartetting wave function approach suggest that, as the α cluster approaches the core nucleus from the infinity, its density profile encounters deformations (or dissolutions) due to the Pauli blocking.

G. Röpke *et al.* (2014).
C. Xu *et al.* (2016, 2017).
D. Deng, Z. Ren (2017).
D. Deng, Z. Ren, N. Wang (2019).

Basic Picture

- At the infinity, the α cluster is identified with the α particle in the vacuum.
- As the α cluster approaches the core nucleus, it starts to sense the Pauli-blocking effect of the core nucleus and the nucleons inside the α cluster are redistributed.
- As the α cluster arrives at the center of the core nucleus, the α-cluster state is "dissolved" (almost) completely and the nucleons occupy the valence orbits of the core nucleus.

The "dissolution" of the α cluster inside infinite nuclear matter and heavy nuclei has been studied microscopically, which shows the importance of the Pauli blocking.

G. Röpke *et al.* (2014).

Alternative: use the Brink wave function to simulate dynamics of the α cluster approaching the finite core nucleus from the infinity.

$$\Psi_{\mathbf{S}}(\{\mathbf{r}_A,\sigma_{Az},\tau_{Az};\mathbf{r}_a,\sigma_{az},\tau_{az}\}) = \mathscr{A}_{Aa}\{\Phi_A(\{\mathbf{r}_A,\sigma_{Az},\tau_{Az}\})\Phi_a(\{\mathbf{r}_a,\sigma_{az},\tau_{az}\},\mathbf{S})\},$$

$$\Phi_A(\{\mathbf{r}_A,\sigma_{Az},\tau_{Az}\}) = \det\{\varphi^{\beta}_{n_1 l_1 m_1 \sigma_1 \tau_1}\cdots\varphi^{\beta}_{n_{A_T} l_{A_T} m_{A_T} \sigma_{A_T} \tau_{A_T}}\}/\sqrt{A_T!},$$

$$\Phi_a(\{\mathbf{r}_a,\sigma_{az},\tau_{az}\},\mathbf{S}) = \det\{\varphi^{\alpha}_{\mathbf{S}\sigma_{A_T+1}\tau_{A_T+1}}\cdots\varphi^{\alpha}_{\mathbf{S}\sigma_{A_T+A_\alpha}\tau_{A_T+A_\alpha}}\}/\sqrt{A_\alpha!},$$

$$\varphi^{\beta}_{n_A l_A m_A \sigma_A \tau_A}(\mathbf{r}_A,\sigma_{Az},\tau_{Az}) = \phi^{\beta}_{n_A l_A m_A}(\mathbf{r}_A)\chi_{\sigma_A}(\sigma_{Az})\xi_{\tau_A}(\tau_{Az}),$$

$$\varphi^{\alpha}_{\mathbf{S}\sigma_a\tau_a}(\mathbf{r}_a,\sigma_{az},\tau_{az}) = \phi_{\mathbf{S}}(\mathbf{r}_a)\chi_{\sigma_a}(\sigma_{az})\xi_{\tau_a}(\tau_{az}),$$

$$\phi_{\mathbf{S}}(\mathbf{r}_a) = (\alpha/\pi)^{3/4}\exp\left[-\alpha(\mathbf{r}_a-\mathbf{S})^2/2\right]. \qquad (8)$$

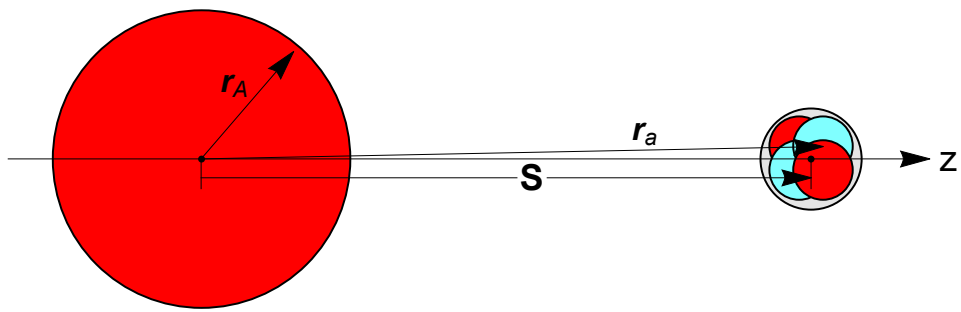

Evolving density profile of the α cluster:

$$\Psi_{\mathbf{S}}(\{\mathbf{r}_A,\sigma_{Az},\tau_{Az};\mathbf{r}_a,\sigma_{az},\tau_{az}\}) = \mathscr{A}_{Aa}\{\Phi_A(\{\mathbf{r}_A,\sigma_{Az},\tau_{Az}\})\Phi_a(\{\mathbf{r}_a,\sigma_{az},\tau_{az}\},\mathbf{S})\},$$

$$\Longrightarrow \Psi_{\mathbf{S}}(\{\mathbf{r}_A,\sigma_{Az},\tau_{Az};\mathbf{r}_a,\sigma_{az},\tau_{az}\}) = \mathscr{A}_{Aa}\{\Phi_A(\{\mathbf{r}_A,\sigma_{Az},\tau_{Az}\})\widetilde{\Phi}_a(\{\mathbf{r}_a,\sigma_{az},\tau_{az}\},\mathbf{S})\},$$

$$\widetilde{\Phi}_a(\{\mathbf{r}_a,\sigma_{az},\tau_{az}\},\mathbf{S}) = \det\{\psi^{\alpha}_{\mathbf{S}\sigma_{A_T+1}\tau_{A_T+1}}\cdots\psi^{\alpha}_{\mathbf{S}\sigma_{A_T+A_\alpha}\tau_{A_T+A_\alpha}}\}/\sqrt{A_\alpha!},$$

$$\psi^{\alpha}_{\mathbf{S}\sigma_a\tau_a}(\mathbf{r}_a,\sigma_{az},\tau_{az}) = \mathcal{N}(\mathbf{S},\sigma_a,\tau_a)\Big[\varphi^{\alpha}_{\mathbf{S}\sigma_a\tau_a}(\mathbf{r}_a,\sigma_{az},\tau_{az}) - \sum_{A=1}^{A_T}\langle\varphi^{\beta}_{n_Al_Am_A\sigma_A\tau_A}|\varphi^{\alpha}_{\mathbf{S}\sigma_a\tau_a}\rangle\,\varphi^{\beta}_{n_Al_Am_A\sigma_A\tau_A}(\mathbf{r}_a,\sigma_{az},\tau_{az})\Big]. \quad (9)$$

Take $^{20}\mathrm{Ne} = \alpha + {}^{16}\mathrm{O}$ as an example:

The width parameters α and β for the α cluster and the target nucleus are determined by fitting the experimental data on the root-mean-square (RMS) charge radii.

Preliminary Results

Evolving density profile of the α cluster:

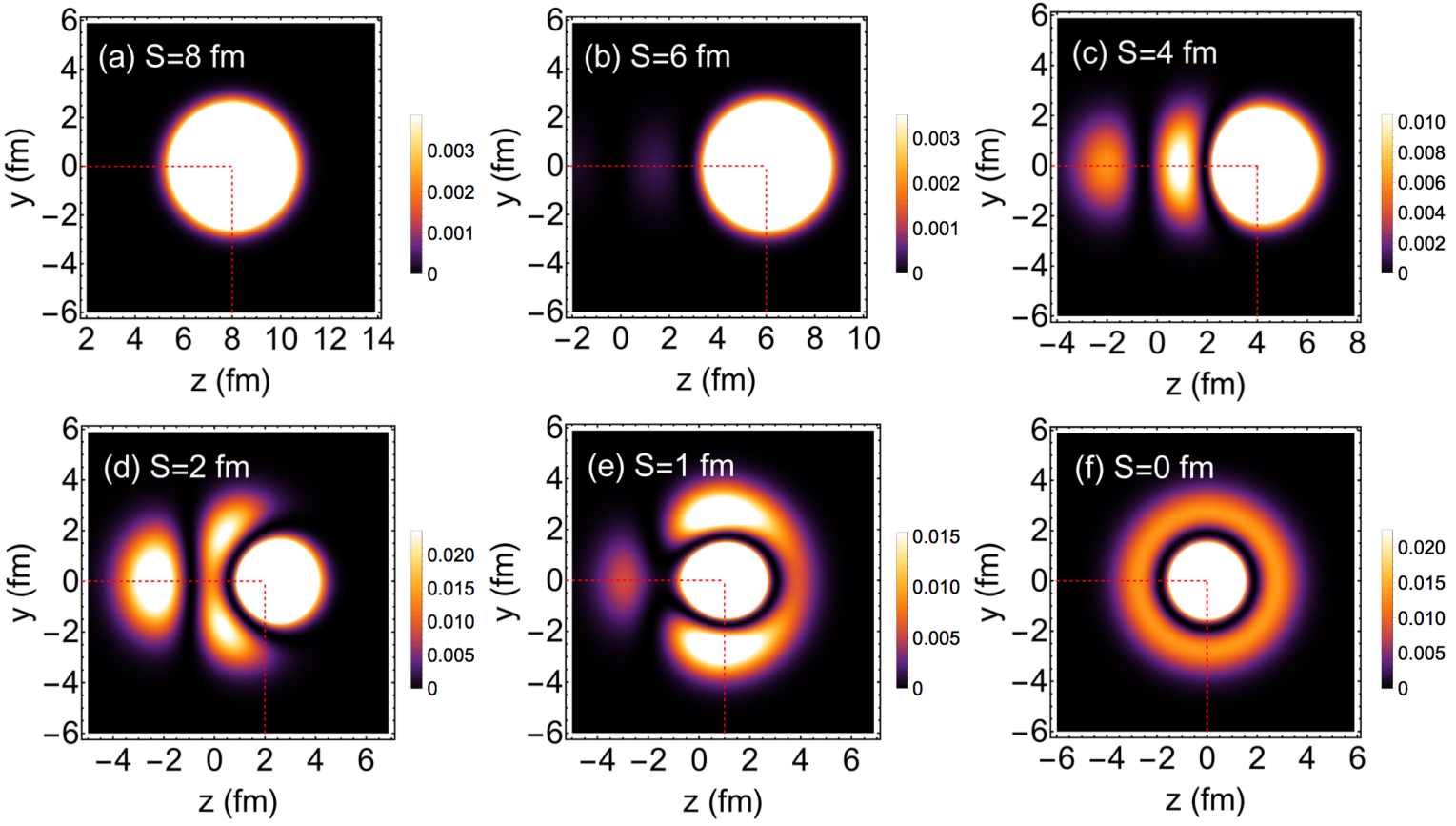

New Double-Folding Potential for the α-^{16}O System

$$W(S) = \int \mathrm{d}\mathbf{r}_A \mathrm{d}\mathbf{r}_a \rho_A(\mathbf{r}_A)\rho_a(\mathbf{r}_a, S) V_{NN}(\mathbf{r}_a - \mathbf{r}_A), \tag{10}$$

$$\text{M3Y}: V_{NN}(r) = 7999\frac{\exp(-4r)}{4r} - 2134\frac{\exp(-2.5r)}{2.5r} - 262\,\delta(\mathbf{r}) + \frac{e^2}{r}. \tag{11}$$

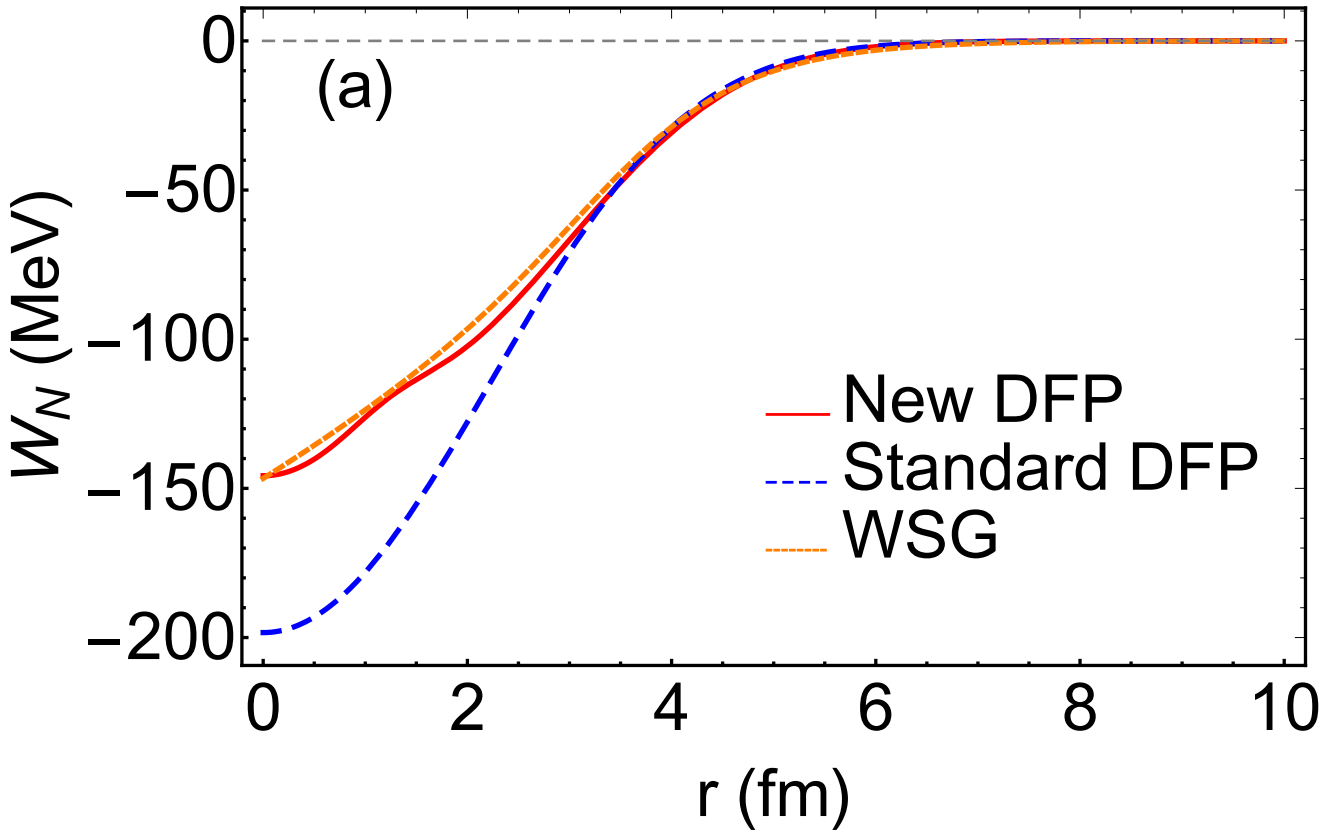

Structural Properties of ^{20}Ne

J^π	E_{exp} [MeV]	$E^{\mathrm{N}}_{\mathrm{th}}$ [MeV]	$E^{\mathrm{S}}_{\mathrm{th}}$ [MeV]	$B(\mathrm{E2}\downarrow)_{\mathrm{exp}}$ [W.u.]	$B(\mathrm{E2}\downarrow)^{\mathrm{N}}_{\mathrm{th}}$ [W.u.]	$B(\mathrm{E2}\downarrow)^{\mathrm{S}}_{\mathrm{th}}$ [W.u.]
0^+	0.000	-1.054	-11.666	–	–	–
2^+	1.634	-0.024	-10.557	20.3 ± 1.0	13.3	6.9
4^+	4.248	3.690	-7.948	22.0 ± 2.0	17.0	8.8
6^+	8.776	4.449	-3.786	20.0 ± 3.0	13.2	7.5
8^+	11.951	7.661	2.016	9.03 ± 1.3	6.8	4.5

The new double-folding potential gives improved results on the structural properties of ^{20}Ne compared with the standard double-folding potential.

α-α Elastic Scattering from Non-Localized Cluster Model

Brink-THSR Wave Function + Calculable R-Matrix Theory

The Brink-THSR wave function is one of mathematical realizations of the non-localized clustering and hybrids the Brink and the THSR wave function

$$\Psi_{\text{Brink-THSR}}(\beta, \mathbf{T}) = \mathscr{N} \int \mathrm{d}^3 R \, \exp\left(-\frac{\mathbf{R}^2}{2\beta^2}\right) \Phi_{\mathrm{B}}(\mathbf{R} + \mathbf{T}). \tag{12}$$

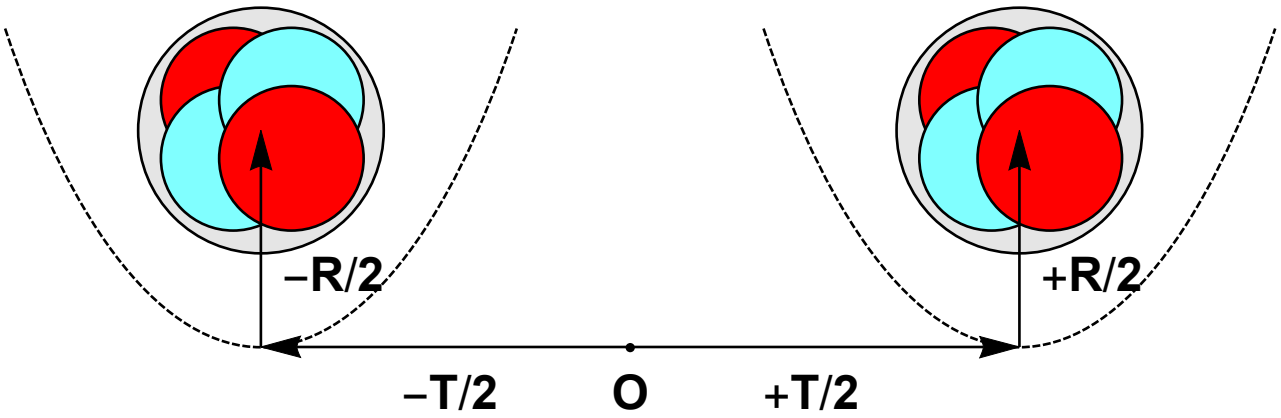

Two containers are localized at the endpoints separated by the generator coordinate $\mathbf{T}$, while the α cluster moves non-locally in the container.

The Brink-THSR wave function in the intrinsic frame is given by

$$\Psi(\beta,\mathbf{T}) = \mathscr{N}\int \mathrm{d}^3R\, \exp\left(-\frac{\mathbf{R}^2}{2\beta^2}\right)\Phi_{\mathrm{B}}(\mathbf{R}+\mathbf{T}),$$

$$\begin{aligned}\Phi_{\mathrm{B}}(\mathbf{R}+\mathbf{T}) = \det\{&\varphi_{0s}(\mathbf{r}_1-\mathbf{R}/2-\mathbf{T}/2)\chi_{\sigma_1\tau_1}\cdots\varphi_{0s}(\mathbf{r}_4-\mathbf{R}/2-\mathbf{T}/2)\chi_{\sigma_4\tau_4}\\ &\times\varphi_{0s}(\mathbf{r}_5+\mathbf{R}/2+\mathbf{T}/2)\chi_{\sigma_5\tau_5}\cdots\varphi_{0s}(\mathbf{r}_8+\mathbf{R}/2+\mathbf{T}/2)\chi_{\sigma_8\tau_8}\}/\sqrt{2\times 8!},\end{aligned}$$

$$\varphi_{0s}(\mathbf{r}\pm\mathbf{R}/2\pm\mathbf{T}/2) = (\pi b^2)^{-3/4}\exp\left[-\frac{(\mathbf{r}\pm\mathbf{R}/2\pm\mathbf{T}/2)^2}{2b^2}\right], \tag{13}$$

which could be further simplified as

$$\begin{aligned}\Psi(\beta,\mathbf{T}) &= \Psi_{\mathrm{CM}}(\mathbf{X}_{\mathrm{CM}})\times\widehat{\Psi}(\beta,\mathbf{T}),\\ \Psi_{\mathrm{CM}}(\mathbf{X}_{\mathrm{CM}}) &= \left(\frac{8}{\pi b^2}\right)^{3/4}\exp\left(-\frac{4\mathbf{X}_{\mathrm{CM}}^2}{b^2}\right),\\ \widehat{\Psi}(\beta,\mathbf{T}) &= \frac{1}{\sqrt{140}}\mathscr{A}_{12}\left[\Gamma(\boldsymbol{\rho},\beta,\mathbf{T})\widehat{\phi}(\alpha_1)\widehat{\phi}(\alpha_2)\right]\\ \Gamma(\boldsymbol{\rho},\beta,\mathbf{T}) &= \left(\frac{2}{\pi}\right)^{3/4}\frac{b^{3/2}}{(b^2+2\beta^2)^{3/2}}\exp\left[-\frac{(\boldsymbol{\rho}-\mathbf{T})^2}{b^2+2\beta^2}\right].\end{aligned} \tag{14}$$

To describe physical states with the definite angular momentum and parity, we consider further the partial-wave expansion of the Brink-THSR wave function

$$\Psi(\beta, \mathbf{T}) = \Psi_{\mathrm{CM}}(\mathbf{X}_{\mathrm{CM}}) \times 4\pi \sum_{LM} \widehat{\Psi}_L(\beta, T) Y_{LM}(\Omega_\rho) Y^*_{LM}(\Omega_T), \tag{15}$$

$$\widehat{\Psi}_L(\beta, T) = \frac{1}{\sqrt{140}} \mathscr{A}_{12} \Gamma_L(\rho, \beta, T) \widehat{\phi}(\alpha_1) \widehat{\phi}(\alpha_2), \tag{16}$$

$$\Gamma_L(\rho, \beta, T) = \left(\frac{2}{\pi}\right)^{3/4} \frac{b^{3/2}}{(b^2 + 2\beta^2)^{3/2}} \exp\left(-\frac{\rho^2 + T^2}{b^2 + 2\beta^2}\right) \mathrm{i}_L\left(\frac{2\rho T}{b^2 + 2\beta^2}\right). \tag{17}$$

Here, $\mathrm{i}_L(x) = \sqrt{\frac{\pi}{2x}} I_{L+1/2}(x)$, with $I_{L+1/2}(x)$ being the modified Bessel function of the first kind.

Calculable R-Matrix Theory

The wave function of the **scattering state** has asymptotic behavior different from the bound state, which has to be handled carefully.

In the **calculable R-matrix theory**, the configuration space is divided into the interior region and the exterior region.

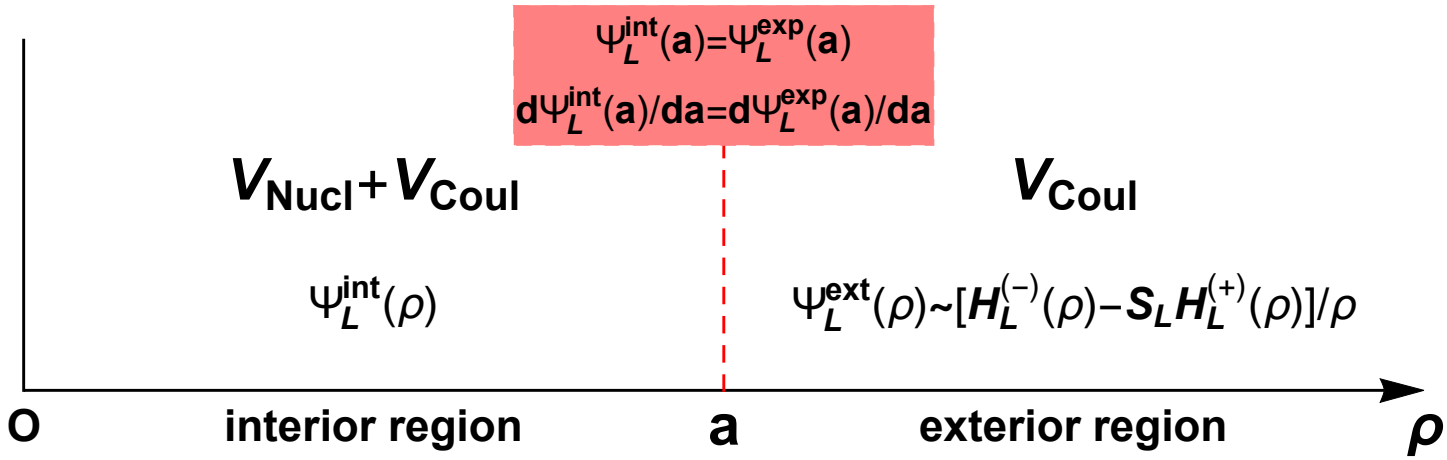

P. Descouvemont and D. Baye, Rept. Prog. Phys. **73**, 036301 (2010).

Bloch-Schrödinger Equation

An elegant way to realize the calculable R-matrix theory is through the Bloch-Schrödinger equation

$$(H_L + \mathcal{L} - E)\Psi_L^{\text{int}} = \mathcal{L}\Psi_L^{\text{ext}}, \tag{18}$$

with $\mathcal{L} = \frac{\hbar^2}{2\mu a}\delta(\rho - a)\frac{\mathrm{d}}{\mathrm{d}\rho}\rho$ being the Bloch operator.

The Hamiltonian H_L is not Hermitian over the interval $\rho \in [0, a]$,

$$\int_0^a \mathrm{d}\rho\, \psi H_L \phi - \int_0^a \mathrm{d}\rho\, \phi H_L \psi = \frac{\hbar^2}{2\mu}[\psi'(a)\phi(a) - \psi(a)\phi'(a)], \tag{19}$$

which is non-vanishing!

This problem is solved with the help of the Bloch operator

$$\int_0^a \mathrm{d}\rho\, \psi(H_L + \mathcal{L})\phi = \int_0^a \mathrm{d}\rho\, \phi(H_L + \mathcal{L})\psi. \tag{20}$$

In the interior region, the wave function $\widehat{\Psi}_L^{\rm int}(E)$ at the reaction energy E (in the CM frame) is given by

$$\widehat{\Psi}_L^{\rm int}(E) = \int {\rm d}T f_L(T)\widehat{\Psi}_L(\beta, T) = \sum_n \widetilde{f}_L(T_n)\widehat{\Psi}_L(\beta, T_n). \qquad (21)$$

In the exterior region, the short-range nuclear interaction and the anti-symmetrization between the two α clusters could be safely neglected. The radial component of the exterior wave function takes the form of

$$\widehat{\Psi}_L^{\rm ext}(E) = g_L^{\rm ext}(\rho)\widehat{\phi}(\alpha_1)\widehat{\phi}(\alpha_2), \qquad (22)$$

$$g_L^{\rm ext}(\rho) = \frac{1}{\rho}\left[\mathcal{H}_L^{(-)}(\eta, k\rho) - \mathcal{S}_L(E)\mathcal{H}_L^{(+)}(\eta, k\rho)\right], \qquad (23)$$

where $\mathcal{H}_L^{(\mp)}(\eta, k\rho)$ are the ingoing/outgoing Coulomb-Hankel functions.

Substituting Eq. (21) into the Bloch-Schrödinger equation, we have

$$\sum_{n'} C_{nn'} \widetilde{f}_L(T_{n'}) = \langle \widehat{\Psi}_I(\beta, T_n) | \mathcal{L} | \widehat{\Psi}_L^{\text{ext}}(E) \rangle \,, \tag{24}$$

$$C_{nn'} = \left(\widehat{\Psi}_L(\beta, T_n) | H_L + \mathcal{L} - E | \widehat{\Psi}_L(\beta, T_{n'}) \right). \tag{25}$$

The round brackets "( )" in Eq. (25) refer to the interior matrix element, which is evaluated within the interior region only.

With the matrix elements $\{C_{nn'}\}$, the R matrix and S matrix are given by

$$\mathcal{R}_L = \frac{\hbar^2 a}{2\mu} \sum_{nn'} \Gamma_L(a, \beta, T_n)(C)^{-1}_{nn'} \Gamma_L(a, \beta, T_{n'}), \tag{26}$$

$$\mathcal{S}_L = \frac{\mathcal{H}_L^{(-)}(\eta, ka) - ka\, \mathcal{H}_L^{(-)'}(\eta, ka)\mathcal{R}_L}{\mathcal{H}_L^{(+)}(\eta, ka) - ka\, \mathcal{H}_L^{(+)'}(\eta, ka)\mathcal{R}_L}, \tag{27}$$

where $\mathcal{H}_L^{(\mp)'}(\eta, ka)$ is the derivative of $\mathcal{H}_L^{(\mp)}(\eta, ka)$ with respect to ka. With the S matrix given in Eq. (27), the interior wave function Ψ_L^{int} could be obtained by solving the linear equations Eq. (24).

Energy Surface

The energy surfaces of the $\alpha + \alpha$ system given by a **single** Brink-THSR wave function

$$E_L(\beta, T) = \frac{\langle \widehat{\Psi}_L(\beta, T) | H_L | \widehat{\Psi}_L(\beta, T) \rangle}{\langle \widehat{\Psi}_L(\beta, T) | \widehat{\Psi}_L(\beta, T) \rangle}.$$

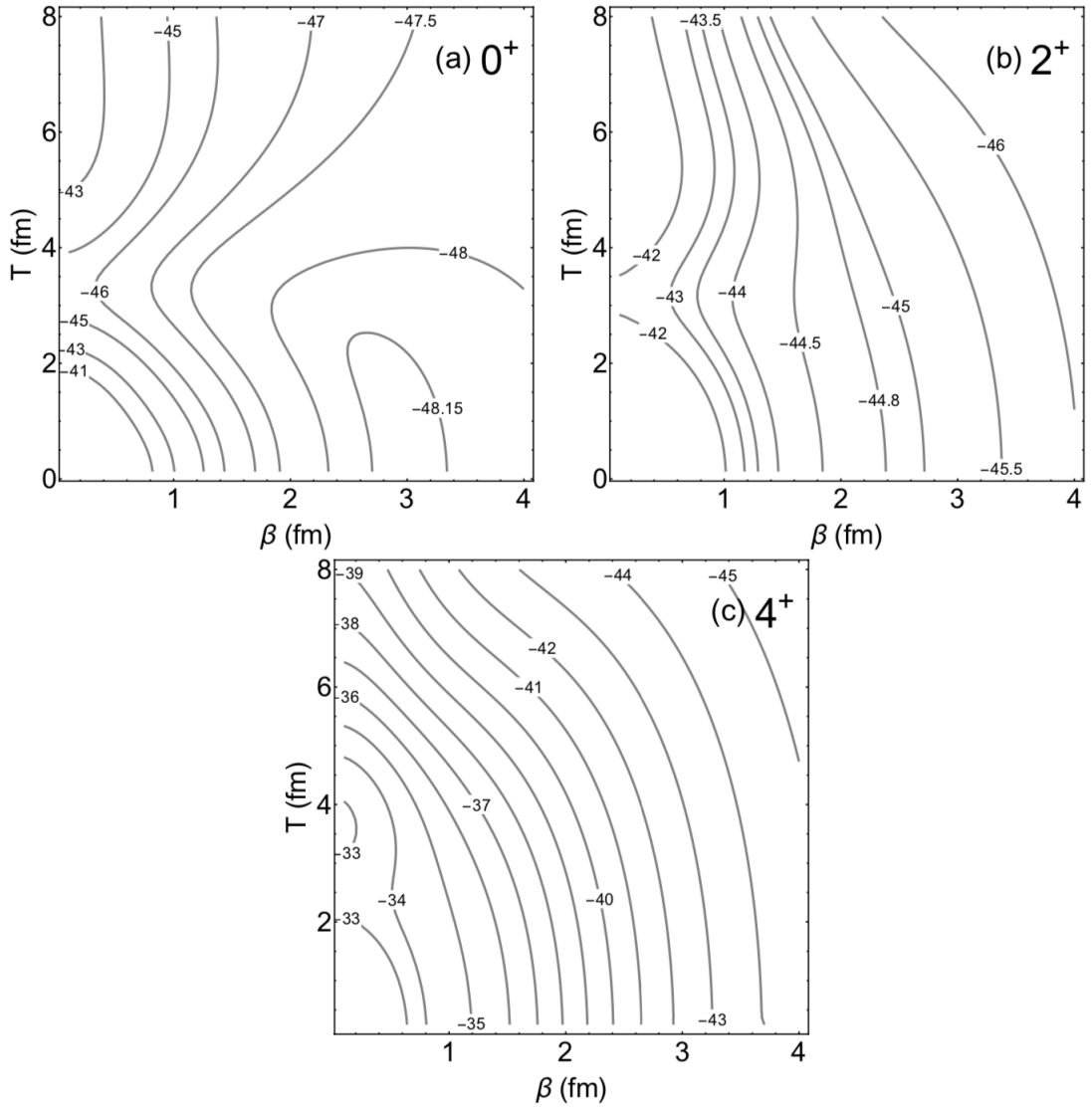

FIG. 3: The energy surface of the 0^+, 2^+, and 4^+ states of ^{8}Be.

Phase Shifts

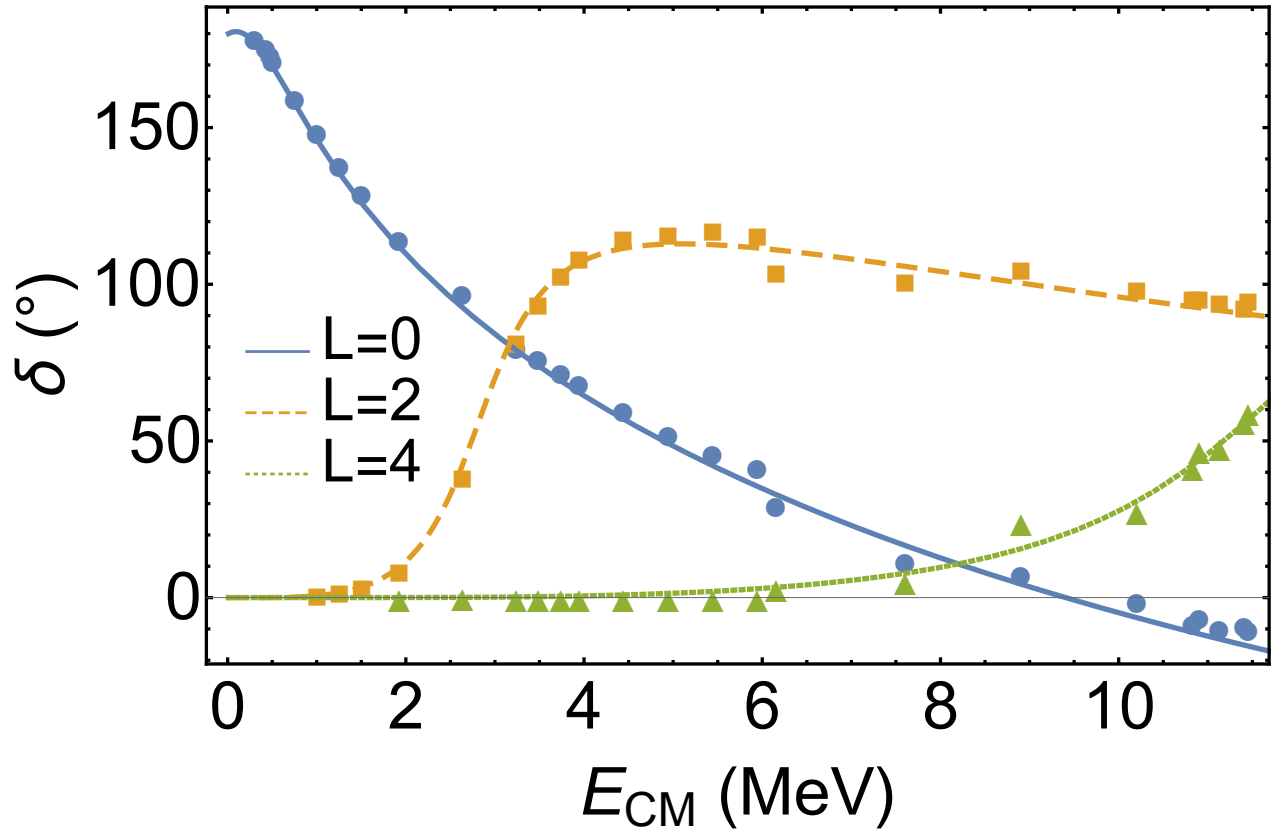

For $\beta = 0,\ 0.5,\ 1$ fm, the non-localized cluster model gives the theoretical results consistent with the experimental data.

Momentum-Space Gaussian Expansion Method and Chiral Potentials

Momentum-Space Gaussian Expansion Method

Gaussian expansion method (GEM) is a theoretical approach to quantum few-body problem developed by Kyushu group (Kamimura, Hiyama, Kino, etc). It solves the few-body Schrödinger equation in the **configuration space** and has been carried out for two-body, three-body, four-body, and five-body systems.

E. Hiyama, Y. Kino, M. Kamimura (2003).
E. Hiyama (2012).
E. Hiyama, M. Kamimura (2018).

Motivation: There are interactions that are given naturally in the momentum space and become non-local in the configuration space, e.g., the chiral potential.

Goal: Extend the GEM from the configuration space to the momentum space. $\Longrightarrow$ Momentum-Space Gaussian Expansion Method (MSGEM).

Jacobi Coordinate in the Momentum Space

$$\boldsymbol{p} = \frac{m_2}{m_1+m_2}\boldsymbol{p}_1 - \frac{m_1}{m_1+m_2}\boldsymbol{p}_2,$$

$$\boldsymbol{P} = \boldsymbol{p}_1 + \boldsymbol{p}_2.$$

Trial Wave Function:

$$\langle \mathbf{p}|LM\rangle = \sum_{N=1}^{N_{max}} c_N\, \phi_L^N(\nu_N; p)\, Y_{LM}(\boldsymbol{n}_p),$$

$$\phi_L^N(\nu_N; p) = \sqrt{(2\pi)^3 \frac{2^{\frac{5}{2}+L}\nu_N^{\frac{3}{2}+L}}{\Gamma(L+\frac{3}{2})}}\, p^L \exp(-\nu_N p^2).$$

Geometric progression:

$\nu_N = 1/s_N^2$, $s_N = s_1 a^{N-1}$,

with $N = 1, \cdots, N_{max}$.

Generalized Eigenvalue Problem:

$$\sum_{N=1}^{N_{max}} \left[(\mathbf{T}_{N'N} + \mathbf{V}_{N'N}) - E\mathbf{N}_{N'N}\right] c_N = 0,$$

$$\mathbf{T}_{N'N} \equiv \langle \nu_{N'}; LM|\, T_2 |\nu_N; LM\rangle\,,$$

$$\mathbf{V}_{N'N} \equiv \langle \nu_{N'}; LM|\, V |\nu_N; LM\rangle\,,$$

$$\mathbf{N}_{N'N} \equiv \langle \nu_{N'}; LM|\nu_N; LM\rangle\,.$$

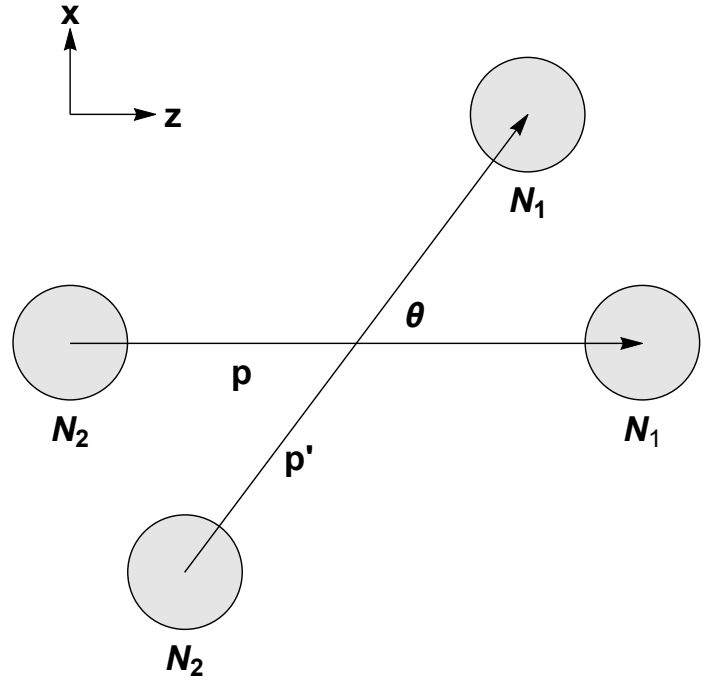

Chiral Potentials

Chiral potentials are based on the **chiral effective field theory**, and relate the dynamics of nucleons and pions to that of quarks and gluons through the **chiral symmetry breaking**.

Main Features:

- UV cutoff $\Lambda \sim 500$ MeV, IR scale $Q \sim m_\pi$;
- power-counting scheme for systematical treatments of chiral and momentum expansions; theoretical uncertainty estimation;
- unified derivation of two-body, three-body, and many-body nuclear forces;
- accurate descriptions of the nucleon-nucleon scattering data with $\chi^2/\text{datum} \sim 1$ at the N^3LO.
- generally non-local in the configuration space, formulated naturally in the momentum space;
- $\cdots$.

The chiral nucleon-nucleon potential is given by

$$V(\boldsymbol{p}', \boldsymbol{p}) = [V_{1\pi}(\boldsymbol{p}', \boldsymbol{p}) + V_{2\pi}(\boldsymbol{p}', \boldsymbol{p}) + V_{ct}(\boldsymbol{p}', \boldsymbol{p}) + \cdots]$$
$$\times f(p', p; n) \times \left(m_N / \sqrt{E_p E_p'} \right)^{n_{MR}} .$$

with $f(p', p; n) = \exp[-(p'/\Lambda)^{2n} - (p/\Lambda)^{2n}]$ being the regulator function, Λ being the cutoff parameter and n being the non-perturbative regularization index.

Leading Order:

$$
\begin{aligned}
V_{LO}^{np}(\boldsymbol{p}',\boldsymbol{p}) &= V_{1\pi}^{np}(\boldsymbol{p}',\boldsymbol{p}) + V_{ct}^{(0)}(\boldsymbol{p}',\boldsymbol{p}) + V_{EM}^{np}(\boldsymbol{p}',\boldsymbol{p}),\\
V_{1\pi}^{np}(\boldsymbol{p}',\boldsymbol{p}) &= -V_{1\pi}(\boldsymbol{p}',\boldsymbol{p},m_{\pi^0}) + 2(-1)^{I+1}V_{1\pi}(\boldsymbol{p}',\boldsymbol{p},m_{\pi^\pm}),\\
V_{1\pi}(\boldsymbol{p}',\boldsymbol{p},m) &= -\frac{g_A^2}{4F_\pi^2}\frac{\boldsymbol{\sigma}_1\cdot\boldsymbol{q}\,\boldsymbol{\sigma}_2\cdot\boldsymbol{q}}{q^2+m^2},\\
V_{ct}^{(0)}(\boldsymbol{p}',\boldsymbol{p}) &= C_S + C_T\,\boldsymbol{\sigma}_1\cdot\boldsymbol{\sigma}_2,\\
V_{EM}^{np}(\boldsymbol{p}',\boldsymbol{p}) &= V_T^\gamma(q)\left[\boldsymbol{\sigma}_1\cdot\boldsymbol{q}\,\boldsymbol{\sigma}_2\cdot\boldsymbol{q} - \frac{1}{3}(\boldsymbol{\sigma}_1\cdot\boldsymbol{\sigma}_2)q^2\right]\\
&\quad - V_{LS}^\gamma(q)\left[-\frac{i}{2}(\boldsymbol{\sigma}_1+\boldsymbol{\sigma}_2)\cdot(\boldsymbol{q}\times\boldsymbol{k})\right]\\
&\quad - V_{LA}^\gamma(q)\left[-\frac{i}{2}(\boldsymbol{\sigma}_1-\boldsymbol{\sigma}_2)\cdot(\boldsymbol{q}\times\boldsymbol{k})\right],
\end{aligned}
$$

$$
V_T^\gamma(q) = \frac{4\pi e^2}{q^2}\frac{\kappa_n\mu_p}{4m_nm_p}, \qquad V_{LS}^\gamma(q) = V_{LA}^\gamma(q) = \frac{4\pi e^2}{q^2}\frac{\kappa_n}{m_nm_N}.
$$

Next-to-Leading Order:

$$V_{NLO}(\boldsymbol{p}',\boldsymbol{p}) = V_{LO}(\boldsymbol{p}',\boldsymbol{p}) + V_{2\pi}^{(2)}(\boldsymbol{p}',\boldsymbol{p}) + V_{ct}^{(2)}(\boldsymbol{p}',\boldsymbol{p}),$$

$$V_{2\pi}^{(2)}(\boldsymbol{p}',\boldsymbol{p}) = W_C^{(2)}(q)\,\boldsymbol{\tau}_1\cdot\boldsymbol{\tau}_2 + V_S^{(2)}(q)\,\boldsymbol{\sigma}_1\cdot\boldsymbol{\sigma}_2 + V_T^{(2)}(q)\,\boldsymbol{\sigma}_1\cdot\boldsymbol{q}\,\boldsymbol{\sigma}_2\cdot\boldsymbol{q},$$

$$W_C^{(2)}(q) = \frac{L(q,\widetilde{\Lambda})}{384\pi^2 F_\pi^4}\left[4m_\pi^2(1+4g_A^2-5g_A^4) + q^2(1+10g_A^2-23g_A^4) - \frac{48g_A^4 m_\pi^4}{\omega^2}\right],$$

$$V_S^{(2)}(q) = \frac{3g_A^4}{64\pi^2 F_\pi^4}\,q^2 L(q,\widetilde{\Lambda}),$$

$$V_T^{(2)}(q) = -\frac{3g_A^4}{64\pi^2 F_\pi^4} L(q,\widetilde{\Lambda}),$$

$$V_{ct}^{(2)}(\boldsymbol{p}',\boldsymbol{p}) = C_1 q^2 + C_2 k^2 + \left(C_3 q^2 + C_4 k^2\right)\boldsymbol{\sigma}_1\cdot\boldsymbol{\sigma}_2 + C_5\left[-\frac{i}{2}(\boldsymbol{\sigma}_1+\boldsymbol{\sigma}_2)\cdot(\boldsymbol{q}\times\boldsymbol{k})\right] + C_6\,\boldsymbol{\sigma}_1\cdot\boldsymbol{q}\,\boldsymbol{\sigma}_2\cdot\boldsymbol{q} + C_7\,\boldsymbol{\sigma}_1\cdot\boldsymbol{k}\,\boldsymbol{\sigma}_2\cdot\boldsymbol{k}.$$

Next-to-Next-to-Leading Order:

$$V_{N^2LO}(\boldsymbol{p}', \boldsymbol{p}) = V_{LO}(\boldsymbol{p}', \boldsymbol{p}) + V_{NLO}(\boldsymbol{p}', \boldsymbol{p}) + V_{2\pi}^{(3)}(\boldsymbol{p}', \boldsymbol{p}).$$

$$V_{2\pi}^{(3)}(\boldsymbol{p}', \boldsymbol{p}) = V_C^{(3)}(q) + W_S^{(3)}(q)\, \boldsymbol{\sigma}_1 \cdot \boldsymbol{\sigma}_2\, \boldsymbol{\tau}_1 \cdot \boldsymbol{\tau}_2$$

$$+ W_T^{(3)}(q)\, \boldsymbol{\sigma}_1 \cdot \boldsymbol{q}\, \boldsymbol{\sigma}_2 \cdot \boldsymbol{q}\, \boldsymbol{\tau}_1 \cdot \boldsymbol{\tau}_2.$$

$$V_C^{(3)}(q) = \frac{3g_A^2}{16\pi F_\pi^4} \left[2m_\pi^2(c_3 - 2c_1) + c_3 q^2\right] (2m_\pi^2 + q^2) A(q, \widetilde{\Lambda}),$$

$$W_S^{(3)}(q) = \frac{g_A^2}{32\pi F_\pi^4} c_4\, \omega^2 q^2 A(q, \widetilde{\Lambda}),$$

$$W_T^{(3)}(q) = -\frac{g_A^2}{32\pi F_\pi^4} c_4\, \omega^2 A(q, \widetilde{\Lambda}).$$

Preliminary Results

MSGEM for Deuteron:

$$\left[\frac{\boldsymbol{p}^2}{m_N} + V - E\right] |JMII_z\rangle = 0,$$

$$\langle \boldsymbol{p}, \{s_{1z}, s_{2z}\}, \{\iota_{1z}, \iota_{2z}\} | JMII_z\rangle = \sum_{N=1}^{N_{max}} c_{NL} \phi_L^N(\nu_N; p) \times [Y_L(\boldsymbol{n}_p)\chi_S(s_{1z}, s_{2z})]_{JM} \xi_{II_z}(\iota_{1z}, \iota_{2z}),$$

Generalized Eigenvalue Problem:

$$\sum_{N=1}^{N_{max}} \sum_{L'} \left[(\boldsymbol{T}^{JSII_z}_{N'L',NL} + \boldsymbol{V}^{JSII_z}_{N'L',NL}) - E\boldsymbol{N}^{JSII_z}_{N'L',NL} \right] c_{NL} = 0,$$

$$\begin{aligned}
\boldsymbol{T}^{JSII_z}_{N'L',NL} &= \langle \nu_{N'}; JMII_z, L'S | T_2 | \nu_N; JMII_z, LS \rangle \\
&= \delta_{L'L}\, m_N^{-1}\, 2^{\frac{1}{2}+L}(3+2L)(\nu_{N'}\nu_N)^{\frac{1}{4}(3+2L)}(\nu_{N'}+\nu_N)^{-\frac{5}{2}-L}, \\
\boldsymbol{V}^{JSII_z}_{N'L',NL} &= \langle \nu_{N'}; JMII_z, L'S | V | \nu_N; JMII_z, LS \rangle, \\
\boldsymbol{N}^{JSII_z}_{N'L',NL} &= \langle \nu_{N'}; JMII_z, L'S | \nu_N; JMII_z, LS \rangle \\
&= \delta_{L'L}\, 2^{\frac{3}{2}+L}(\nu_{N'}\nu_N)^{\frac{1}{4}(3+2L)}(\nu_{N'}+\nu_N)^{-\frac{3}{2}-L}.
\end{aligned}$$

Take the Göteborg-Tennessee realization of the chiral potential up to the N^2LO,

- the MR switch-off/on parameter $n_{MR} = 1$,
- the SFR cut-off $\widetilde{\Lambda} = 700$ MeV,
- the non-perturbative regularization index $n = 3$,
- the non-perturbative regularization cut-off $\Lambda = 500$ MeV.

B. D. Carlsson, A. Ekström, C. Forssen, D. Fahlin Strömberg, G. R. Jansen, O. Lilja, M. Lindby, B. A. Mattsson, K. A. Wendt (2016).

	E_{MSGEM} (MeV)	E_{MB} (MeV)
LO	-2.206	-2.208
NLO	-2.211	-2.219
N^2LO	-2.221	-2.222

Conclusions

1. New Double-Folding Potential from the Brink Wave Function
   - robustness with different M3Y effective potentials,
   - improve harmonic-oscillator shell-model description of the core nucleus,
   - extend to heavier nucleus.
2. α-α Elastic Scattering from Non-Localized Cluster Model
   - container evolution in nuclear reaction.

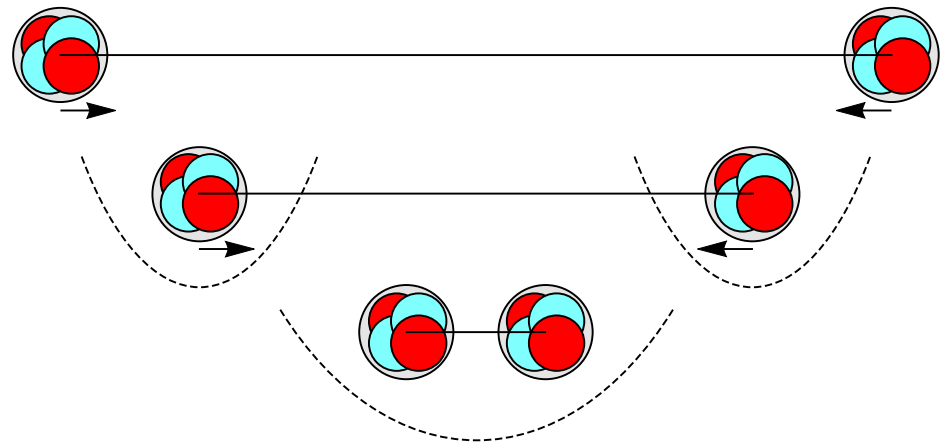

3. Momentum-Space Gaussian Expansion Method and Chiral Potentials
   - Deuteron properties at unphysical pion mass,
   - Triton, ^{3}He, ^{4}He.

Thanks!